LAWRENCE
LIVERMORE
NATIONAL
LABORATORY

UCRL-CONF-232607

The Corrosion Resistance of Fe-Based Amorphous Metals: Fe49.7Cr17.7Mn1.9Mo7.4W1.6B15.2C3.8Si2. and Other Compositions

J. Farmer, J. Haslam, S. Day, T. Lian, C-K. Saw, P. Hailey, J-S. Choi, R. Rebak, J. Payer, C. Blue, W. Peters, D. Branagan

July 10, 2007

Materials Science & Technology 2007 Conference and Exhibition
Detroit, MI, United States
September 16, 2007 through September 20, 2007

The Corrosion Resistance of Fe-Based Amorphous Metals: $Fe_{49.7}Cr_{17.7}Mn_{1.9}Mo_{7.4}W_{1.6}B_{15.2}C_{3.8}Si_{2.4}$ and Other Compositions

J. Farmer, J. Haslam, S. Day, T. Lian, C-K. Saw, P. Hailey, J-S. Choi and R. Rebak
Lawrence Livermore National Laboratory, Livermore, California USA

J. Payer
Case Western Reserve University, Cleveland, Ohio USA

C. Blue and W. Peters
Oak Ridge National Laboratory, Oak Ridge, Tennessee USA

D. Branagan
The NanoSteel Company, Idaho Falls, Idaho USA

Keywords: Iron-Based, Amorphous Metal, Corrosion Resistance, Cyclic Voltammetry

Abstract

Several Fe-based amorphous metals were developed with good corrosion resistance. These materials have been produced as melt-spun ribbons, ingots, and thermal-spray coatings. Cyclic polarization has been conducted in several aggressive environments, at ambient temperature, as well as temperatures approaching the boiling points of the test solutions. The hypothesis that the corrosion resistance of iron-based amorphous metals can be enhanced through application of heuristic principles related to the additions of chromium, molybdenum, tungsten has been tested and found to have merit. Chromium (Cr), molybdenum (Mo) and tungsten (W) provide corrosion resistance; boron (B) enables glass formation; and rare earths such as yttrium (Y) lower critical cooling rate (CCR). The high boron content of this particular amorphous metal makes this amorphous alloy an effective neutron absorber, and suitable for criticality control applications. In general, the corrosion resistance of such iron-based amorphous metals is maintained at operating temperatures up to the glass transition temperature.

.

Introduction

The outstanding corrosion that may be possible with amorphous metals was recognized several years ago [1-3]. Compositions of several iron-based amorphous metals were published, including several with very good corrosion resistance. Examples included: thermally sprayed coatings of Fe-10Cr-10-Mo-(C,B), bulk Fe-Cr-Mo-C-B, and Fe-Cr-Mo-C-B-P [4-6]. The corrosion resistance of an iron-based amorphous alloy with yttrium (Y), $Fe_{48}Mo_{14}Cr_{15}Y_2C_{15}B_6$ was also been established [7-9]. Yttrium was added to this alloy to lower the critical cooling rate. Several nickel-based amorphous metals have been developed that exhibit exceptional corrosion performance in acids, but have not been included in this study, which is restricted to Fe-based materials. Very good thermal spray coatings of nickel-based crystalline coatings were deposited with thermal spray, but appear to have less corrosion resistance than nickel-based amorphous metals [10].

A family of iron-based amorphous metals with very good corrosion resistance was developed that can be applied as a protective thermal spray coating. Several promising formulations within this alloy family were formed by addition chromium (Cr), molybdenum (Mo), and tungsten (W) for enhanced corrosion resistance, and boron (B) to enable glass formation and neutron absorption. One of the parent alloys for preparing this series of amorphous alloys is known as SAM40 ($Fe_{52.3}Cr_{19}Mn_2Mo_{2.5}W_{1.7}B_{16}C_4Si_{2.5}$) and was originally developed by Branagan [11-12]. Compositions explored during this study include: SAM35 ($Fe_{54.5}Mn_2Cr_{15}Mo_2W_{1.5}B_{16}C_4Si_5$); SAM40 ($Fe_{52.3}Mn_2Cr_{19}Mo_{2.5}W_{1.7}B_{16}C_4Si_{2.5}$); SAM2X5 ($Fe_{49.7}Cr_{17.7}Mn_{1.9}Mo_{7.4}W_{1.6}B_{15.2}C_{3.8}Si_{2.4}$); SAM6 ($Fe_{43}Cr_{16}Mo_{16}B_5C_{10}P_{10}$); SAM7 or SAM1651 ($Fe_{48}Mo_{14}Cr_{15}Y_2C_{15}B_6$); and SAM10 ($Fe_{57.3}Cr_{21.4}Mo_{2.6}W_{1.8}B_{16.9}$).

As pointed out in the literature, an estimate of the relative pitting resistance of alloys can be made using the pitting resistance equivalence number (PREN), which is calculated using the elemental composition of the alloy [13-18]. PREN values for the Fe-based amorphous metals of interest here, and the crystalline reference materials, which include Type 316L stainless steel and Ni-based Alloy C-22, have been calculated using the following equations. Equation 1 has been used for estimating the PREN for nickel-based alloys, and accounts for the beneficial effects of Cr, Mo, W and N on corrosion resistance [15].

$$PREN = [\%Cr] + 3.3 \times [\%Mo + \%W] + 30 \times [\%N] \quad (1)$$

However, this equation was used to predict comparable corrosion resistance for Alloys C-276 and Alloy C-22, while Alloy C-22 was known to be more corrosion resistant. An equation that has been used to make reasonable predictions of the relative corrosion resistance of austenitic stainless steels and nickel-based alloys such as Alloy C-22 is [16].

$$PREN = [\%Cr] + 3.3 \times \left([\%Mo] + 0.5 \times [\%W]\right) + k \times [\%N] \quad (2)$$

The factor *k* is an adjustable parameter used to account for the beneficial effects of nitrogen. Reasonable values of the factor *k* range from 12.8 to 30, with 16 being accepted as a reasonable value [17]. Estimates used to guide this alloy development were based on the assumption that the value of *k* is 16. PREN values calculated with Equation 2 indicated that the resistance of the SAM2X5 and SAM1651 amorphous metal formulations should be more resistant to localized corrosion than Type 316L stainless steel or nickel-based Alloy C-22. As in the case of crystalline Fe-based and Ni-based alloys, it was found experimentally that the addition of Cr, Mo, and W substantially increased the corrosion resistance of these amorphous alloys. Additional passive film stability may have been observed, which cannot be attributed to composition alone, and may be attributable to the glassy structure. Additional work is required to further understand the relative roles of composition and crystalline structure in high-performance amorphous metal coatings, such as the ones discussed here. An obvious deficiency associated with the use of a parameter based on chemical composition alone to assess the relative corrosion resistance of both crystalline and amorphous alloys is that microstructural effects on passive film breakdown are ignored. The lack of crystalline structure is believed to be a key attribute of corrosion resistant amorphous metals.

Compositions with high concentrations of boron and good corrosion resistance, such SAM2X5, may benefit applications such as the long-term storage of spent nuclear fuel with enhanced criticality safety [19-22]. In regard to such high temperature applications, it has been

shown that the corrosion resistance of such iron-based amorphous metals is maintained at operating temperatures up to the glass transition temperature [19-20]. The upper operating temperature for such materials is believed to be about 570°C ($T_g \approx 579$°C). Above the crystallization temperature ($T_x \approx 628$°C), deleterious crystalline phases formed, and the corrosion resistance was lost.

Experimental

Melt Spun Ribbons

Maximum cooling rates of one million Kelvin per second (10^6 K/s) have been achieved with melt spinning, which is an ideal process for producing amorphous metals over a very broad range of compositions. This process was used to synthesize completely amorphous, Fe-based, corrosion-resistant alloys with near theoretical density, and thereby enabled the effects of coating morphology on corrosion resistance to be separated from the effects of elemental composition. The melt-spun ribbon (MSR) samples produced with this equipment were several meters long, several millimeters wide and approximately 150 microns thick.

Thermal Spray Coatings

The coatings discussed here were made with the high-velocity oxy-fuel (HVOF) process, which involves a combustion flame, and is characterized by gas and particle velocities that are three to four times the speed of sound (mach 3 to 4). This process is ideal for depositing metal and cermet coatings, which have typical bond strengths of 5,000 to 10,000 pounds per square inch (5-10 ksi), porosities of less than one percent (< 1%) and extreme hardness. The cooling rate that can be achieved in a typical thermal spray process such as HVOF are on the order of ten thousand Kelvin per second (10^4 K/s), and are high enough to enable many alloy compositions to be deposited above their critical cooling rates, thereby maintaining the vitreous state. However, the range of amorphous metal compositions that can be processed with HVOF is more restricted than those that can be produced with melt spinning, due to the differences in achievable cooling rates. Both kerosene and hydrogen have been investigated as fuels in the HVOF process used to deposit SAM2X5.

X-Ray Diffraction

The basic theory for X-ray diffraction (XRD) of amorphous materials is well developed and has been published in the literature [23-24]. In an amorphous material, there are broad diffraction peaks. During this study, XRD was done with CuK_α X-rays, a graphite analyzing crystal, and a Philips vertical goniometer, using the Bragg-Bretano method. The X-ray optics were self-focusing, and the distance between the X-ray focal point to the sample position was equal to the distance between the sample position and the receiving slit for the reflection mode. Thus, the intensity and resolution were optimized. Parallel vertical slits were added to improve the scattering signal. Step scanning was performed from 20 to 90° (2θ) with a step size of 0.02° at 4 to 10 seconds per point, depending on the amount of sample. The samples were loaded into a low-quartz holder because the expected intensity was very low, thus requiring that the background scattering be minimized.

Cyclic Polarization

The resistance to localized corrosion is quantified through measurement of the open-circuit corrosion potential (E_{corr}), the breakdown or critical potential ($E_{critical}$), and the repassivation potential (E_{rp}). Spontaneous breakdown of the passive film and localized corrosion require that the open-circuit corrosion potential exceed the critical potential:

$$E_{corr} \geq E_{critical} \tag{2}$$

The greater the difference between the open-circuit corrosion potential and the critical potential ($\Delta E = E_{critical} - E_{corr}$), the more resistant a material is to modes of localized corrosion such a pitting and crevice corrosion. In integrated corrosion models, general corrosion is invoked when E_{corr} is less than $E_{critical}$ ($E_{corr} < E_{critical}$), and localized corrosion is invoked when E_{corr} exceeds $E_{critical}$. Measured values of the repassivation potential (E_{rp}) are sometimes used as conservative estimates of the critical potential ($E_{critical}$).

Different bases exist for determining the critical potential from electrochemical measurements. The breakdown or critical potential has been defined as the potential where the passive current density increases to a level between 1 to 10 $\mu A/cm^2$ (10^{-6} to 10^{-5} A/cm^2) while increasing potential in the positive (anodic) direction during cyclic polarization or potential-step testing. The repassivation potential has been defined as the potential where the current density drops to a level indicative of passivity, which has been *assumed* to be between 0.1 to 1.0 $\mu A/cm^2$ (10^{-7} to 10^{-6} A/cm^2), while decreasing potential from the maximum level reached during cyclic polarization or potential-step testing [13-14, 25]. An alternative definition of the repassivation potential is the potential during cyclic polarization where the forward and reverse scans intersect, a point where the measured current density during the reverse scan drops to a level *known* to be indicative of passivity.

Cyclic polarization (CP) measurements was based on a procedure similar to ASTM (American Society for Testing and Materials) G-5 and other similar standards, with slight modification [26-27]. The ASTM G-5 standard calls for a 1N H_2SO_4 electrolyte, whereas synthetic bicarbonate, sulfate-chloride, chloride-nitrate, and chloride-nitrate solutions, with sodium, potassium and calcium cations, as well as natural seawater were used for this investigation. The natural seawater used in these tests was obtained directly from Half Moon Bay along the northern coast of California. Furthermore, the ASTM G-5 standard calls for the use of de-aerated solutions, whereas aerated and de-aerated solutions were used here. In regard to current densities believed to be indicative of passivity, all data were interpreted in a manner consistent with the published literature.

Temperature-controlled borosilicate glass (Pyrex) electrochemical cells were used for cyclic polarization and other similar electrochemical measurements. Each cell had three electrodes, a working electrode (test specimen), a reference electrode, and a counter electrode. A standard silver silver-chloride electrode, filled with near-saturation potassium chloride solution, was used as the reference, and communicated with the test solution via a Luggin probe placed in close proximity to the working electrode, which minimized Ohmic losses. The electrochemical cell was equipped with a water-cooled junction to maintain the reference electrode at ambient temperature, which thereby maintained integrity of the potential measurement, and with a water-cooled condenser, which prevented the loss of volatile species from the electrolyte.

Results

X-ray diffraction (XRD) of Fe-based amorphous-metal melt-spun ribbon (MSR) samples is shown in Figure 1. These data show amorphous structure, with the absence of crystalline phases known to be detrimental to corrosion performance.

Cyclic Polarization (CP) data for three Fe-based amorphous-metal MSR samples in 5M $CaCl_2$ at 105°C, including SAM27, SAM2X5, and SAM40, are given in Figure 2. The SAM2X5 has enhanced Mo concentration. MSR samples with higher Mo content have superior corrosion performance. A comparison of differences between the observed repassivation potential and corrosion potential for various MSR samples of Fe-based amorphous metal in natural seawater at 90°C, deduced from cyclic polarization data, is given in Figure 3. Similarly, a comparison for samples in natural seawater at 30°C is given in Figure 4. A comparison of differences between the observed repassivation potential and corrosion potential for MSR samples of Fe-based amorphous metal in 5M $CaCl_2$ at 105°C is given in Figure 5. Data for other alloys and non-MSR amorphous metal samples are provided in these figures for comparison.

CP data for two different forms of SAM2X5 in 5M $CaCl_2$ at 105°C are given in Figure 6. The SAM2X5 samples tested included a full-density MSR sample and an early HVOF coating, with partial devitrification. Similarly, CP data for two forms of SAM1651 in natural seawater (SW) at 90°C are given in Figure 7. The SAM1651 samples tested included a full-density MSR sample, and an early HVOF coating, with possible partial devitrification. In general, the MSR samples exhibit better passive film stability than the early HVOF coatings with partial devitrification.

CP data for three Fe-based amorphous-metal HVOF coating samples in natural seawater at 90°C are given in Figure 8. The coating compositions evaluated included: SAM40XV, SAM1651, and SAM2X5. In the case of heated seawater, the SAM2X5 coating, which has enhanced Mo concentration, had the best corrosion performance.

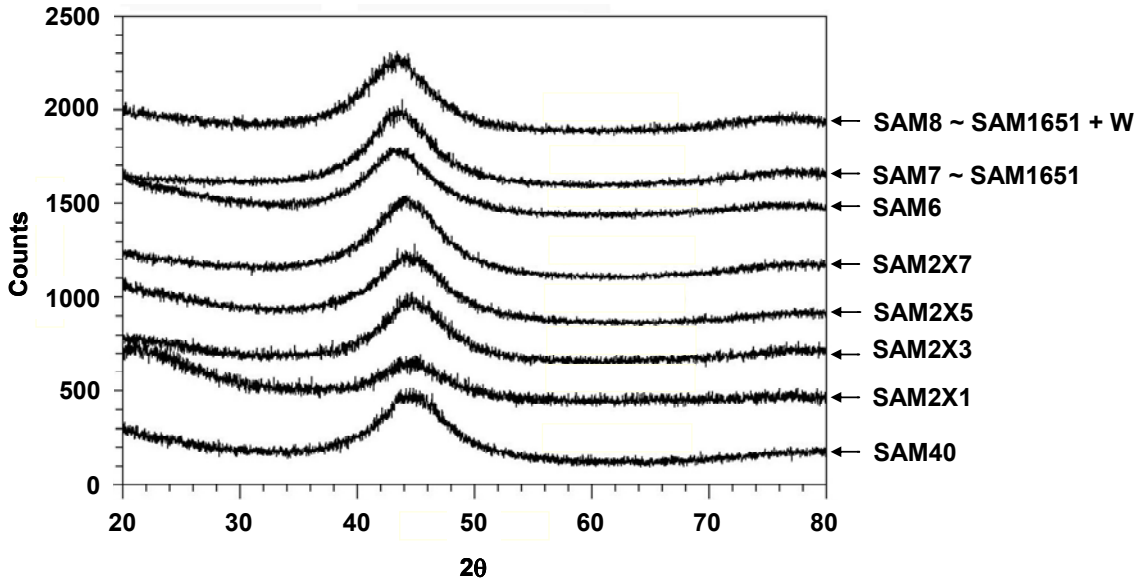

Figure 1. XRD of Fe-based amorphous-metal MSR samples shows amorphous structure, with the absence of crystalline phases known to be detrimental to corrosion performance.

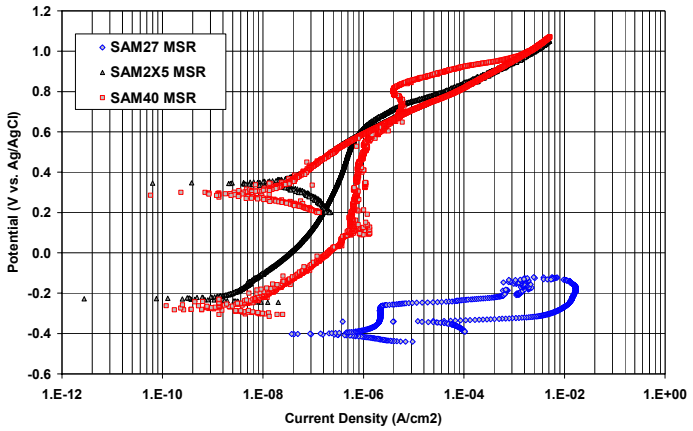

Figure 2. CP of three Fe-based amorphous-metal MSR samples in 5M $CaCl_2$ at 105℃: SAM27, SAM2X5, and SAM40. The SAM2X5 has enhanced Mo concentration. MSR samples with higher Mo content have superior corrosion performance.

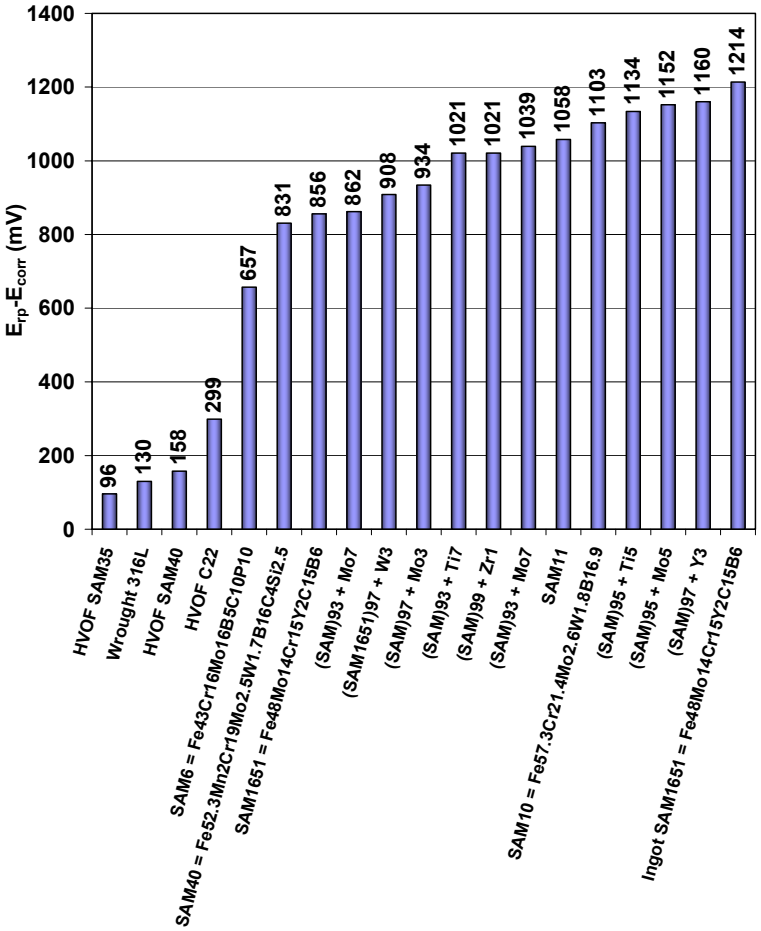

Figure 3. Comparison of differences between the observed repassivation potential and corrosion potential for various MSR samples of Fe-based amorphous metal in natural seawater at 90℃, deduced from cyclic polarization data. Other alloys and non-MSR amorphous metal samples are provided for comparison.

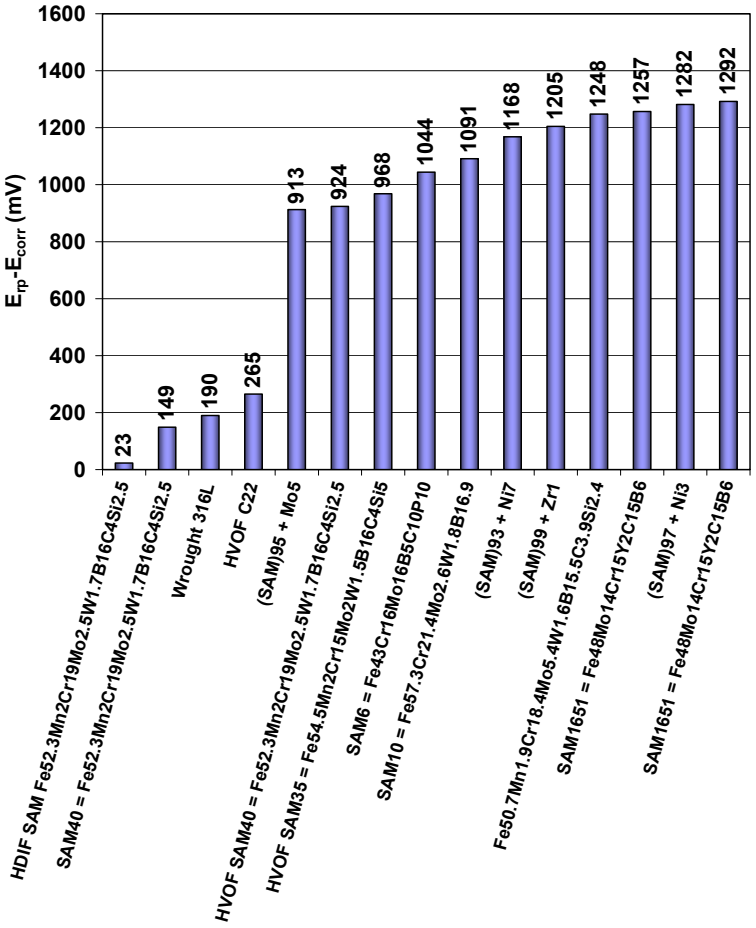

Figure 4. Comparison of differences between the observed repassivation potential and corrosion potential for MSR samples of Fe-based amorphous metal in natural seawater at 30℃, deduced from cyclic polarization data. Other alloys and non-MSR amorphous metal samples are provided for comparison.

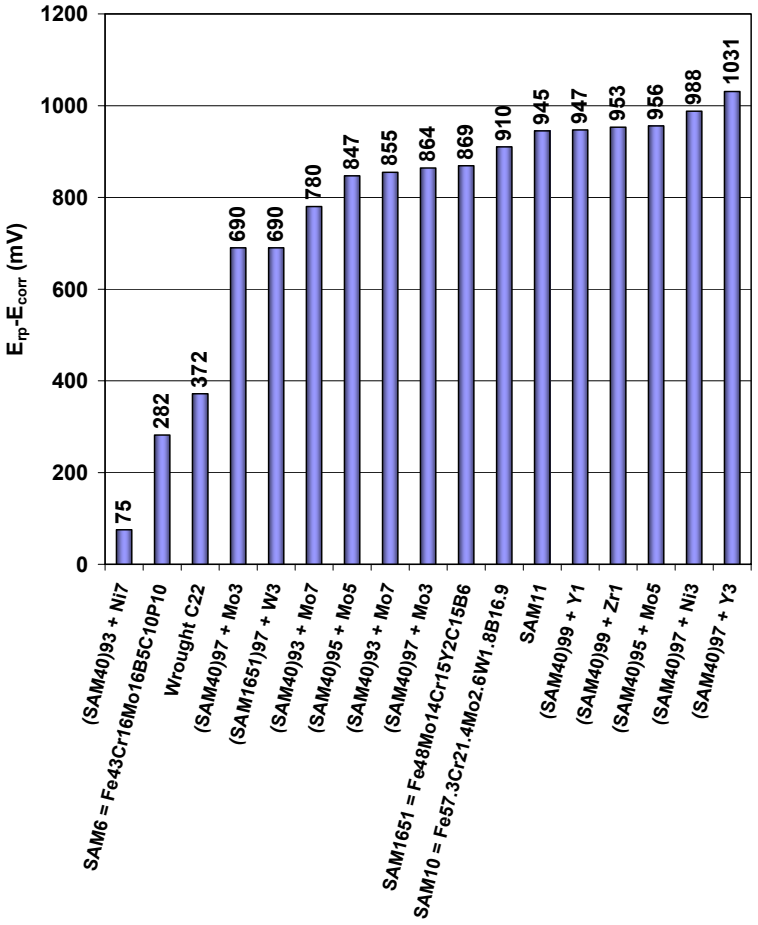

Figure 5. Comparison of differences between the observed repassivation potential and corrosion potential for MSR samples of Fe-based amorphous metal in 5M $CaCl_2$ at 105°C, deduced from cyclic polarization data. Other alloys and non-MSR amorphous metal samples are provided for comparison.

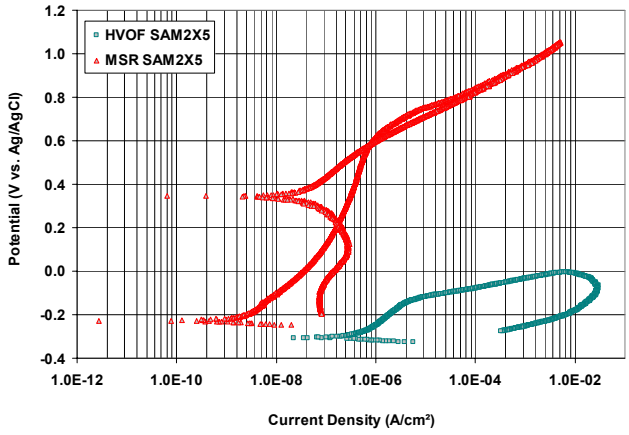

Figure 6. CP of two different forms of SAM2X5 in 5M $CaCl_2$ at 105°C including a full-density MSR sample, and an early HVOF coating, with partial devitrification. The MSR sample exhibited better passive film stability than the early HVOF coating with partial devitrification.

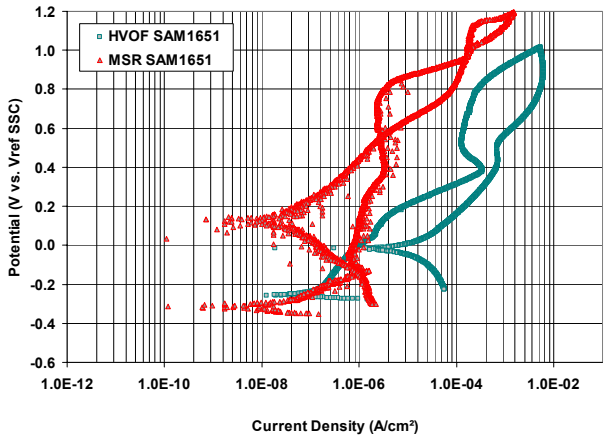

Figure 7. CP of two forms of SAM1651 in natural seawater (SW) at 90°C including a full-density MSR sample, and an early HVOF coating with possible partial devitrification. The MSR samples exhibited better passive film stability than the early HVOF coating with partial devitrification.

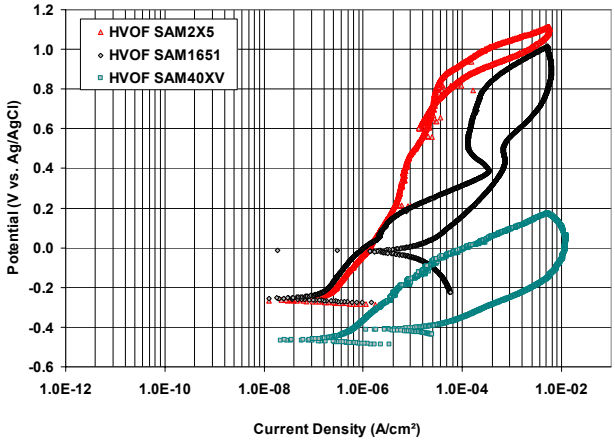

Figure 8. CP of three Fe-based amorphous-metal HVOF coating samples in natural seawater at 90°C: SAM40XV, SAM1651, and SAM2X5. In the case of heated seawater, the SAM2X5 coating, which has enhanced Mo concentration, had the best corrosion performance.

Conclusions

The hypothesis that the corrosion resistance of iron-based amorphous metals can be enhanced through application of heuristic principles related to the additions of chromium, molybdenum, tungsten has been tested with $Fe_{49.7}Cr_{17.7}Mn_{1.9}Mo_{7.4}W_{1.6}B_{15.2}C_{3.8}Si_{2.4}$ (SAM2X5) and found to have merit. Electrochemical tests show that passive film stability superior to that of Type 316L stainless steel and comparable to that of Alloy C-22 can be achieved with iron-based amorphous metals in natural seawater at 30 and 90°C. The passive film on nickel-based Alloy C-22 started to destabilize at approximately 900 mV vs. OCP. The passive films on melt-spun ribbons of SAM2X5 maintained stability at applied potentials greater than 1500 mV vs. OCP, with destabilization observed at 1600 mV.

The passive film stability and corrosion resistance found with iron-based amorphous metals depends upon the form being tested. For example, melt-spun ribbons and ingots have been found to have better passive film stability and corrosion resistance than thermal spray coatings. No significant level of Cr_2B, WC, $M_{23}C_6$ and bcc ferrite was detected in the melt spun ribbons, whereas distinct peaks representing these crystalline phases were observed in the XRD of thermal spray coatings.

Acknowledgments

This work was done under the auspices of the U.S. DOE by Lawrence Livermore National Laboratory (LLNL) under Contract No. W-7405-Eng-48. Work was sponsored by the United States Department of Energy (DOE), Office of Civilian and Radioactive Waste Management (OCRWM); and Defense Advanced Research Projects Agency (DARPA), Defense Science Office (DSO). The guidance of Leo Christodoulou at DARPA DSO and of Jeffrey Walker at DOE OCRWM is gratefully acknowledged.

.

References

[1] M. Telford, The Case for Bulk Metallic Glass. *Materials Today*, Vol. 3, 2004, pp. 36-43

[2] N. Sorensen and R. Diegle, Corrosion of Amorphous Metals, *Corrosion, Metals Handbook*, 9th Ed., Vol. 13, edited by J. R. Davis and J. D. Destefani, ASME, 1987, pp. 864-870

[3] D. Polk and B. Giessen, Overview of Principles and Applications, Chapter 1, *Metallic Glasses*, edited by J. Gilman and H. Leamy, ASME, 1978, pp. 2-35

[4] K. Kishitake, H. Era, and F. Otsubo, Characterization of Plasma Sprayed Fe-10Cr-10Mo-(C,B) Amorphous Coatings, *J. Thermal Spray Tech.*, Vol. 5 (No. 2), 1996, pp. 145-153

[5] S. Pang, T. Zhang, K. Asami, and A. Inoue, Effects of Chromium on the Glass Formation and Corrosion Behavior of Bulk Glassy Fe-Cr-Mo-C-B Alloys, *Materials Transactions*, Vol. 43 (No. 8), 2002, pp. 2137-2142

[6] S. Pang, T. Zhang, K. Asami, and A. Inoue, Synthesis of Fe-Cr-Mo-C-B-P Bulk Metallic Glasses with High Corrosion Resistance, *Acta Materialia*, Vol. 50, 2002, pp. 489-497

[7] F. Guo, S. Poon, and G. Shiflet, Metallic Glass Ingots Based on Yttrium, *Metallic Applied Physics Letters*, Vol. 83 (No. 13), 2003, pp. 2575-2577

[8] Z. Lu, C. Liu, and W. Porter, Role of Yttrium in Glass Formation of Fe-Based Bulk Metallic Glasses, *Metallic Applied Physics Letters*, Vol. 83 (No. 13), 2003, pp. 2581-2583

[9] V. Ponnambalam, S. Poon, and G. Shiflet, *JMR*, Vol. 19 (No. 5), 2004, pp. 1320

[10] D. Chidambaram, C. Clayton, and M. Dorfman, Evaluation of the Electrochemical Behavior of HVOF-Sprayed Alloy Coatings, *Surface and Coatings Technology*, Vol. 176, 2004, pp. 307-317

[11] D. Branagan, Method of Modifying Iron-Based Glasses to Increase Crystallization Temperature Without Changing Melting Temperature, U.S. Pat. Appl. No. 20040250929, Filed Dec. 16, 2004

[12] D. Branagan, Properties of Amorphous/Partially Crystalline Coatings. U.S. Pat. Appl. No. 20040253381, Filed Dec. 16, 2004

[13] H. Hack, Crevice Corrosion Behavior of Molybdenum-Containing Stainless Steel in Seawater, *Materials Performance*, Vol. 22 (No. 6), 1983, pp. 24–30

[14] A. Asphahani, Corrosion Resistance of High Performance Alloys, *Materials Performance*, Vol. 19 (No. 12), 1980, pp. 33–43

[15] R. Rebak and P. Crook, Improved Pitting and Crevice Corrosion Resistance of Nickel and Cobalt Based Alloys, *Symposium on Critical Factors in Localized Corrosion III, 194th ECS Meeting*, Vol. 98-17, 1999, pp. 289-302.

[16] Z. Szklarska-Smialowska, Pitting Resistance Equivalence Number, Effect of Alloying Elements on Stainless Steels and Ni-Base Alloys, Chapter 13, *Pitting and Crevice Corrosion*, NACE, 2005, p. 318-321.

[17] A. Sedriks, Introduction, Pitting, Chapter 4, *Corrosion of Stainless Steels*, J. Wiley & Sons, New York, NY, 1996, p. 111-113

[18] D. Agarwal and M. Kohler, Alloy 33, A New Material Resisting Marine Environment, Paper 424, *Corrosion 97*, NACE, 1997

[19] J. Farmer, J. Haslam, S. Day, T. Lian, C. Saw, P. Hailey, J. Choi, N. Yang, C. Blue, W. Peter, J. Payer and D. Branagan, Corrosion Resistances of Iron-Based Amorphous Metals with Yttrium and Tungsten Additions in Hot Calcium Chloride Brine and Natural Seawater, $Fe_{48}Mo_{14}Cr_{15}Y_2C_{15}B_6$ and W-containing Variants, *Critical Factors in Localized Corrosion 5, A Symposiun in Honor of Hugh Issacs, 210th ECS Meeting*, edited by N. Missert, ECS Transactions, Vol. 3, ECS, 2006

[20] J. Farmer, J. Haslam, S. Day, T. Lian, C. Saw, P. Hailey, J. Choi, R. Rebak, N. Yang, R. Bayles, L. Aprigliano, J. Payer, J. Perepezko, K. Hildal, E. Lavernia, L. Ajdelsztajn, D. Branagan and M. Beardsely, A High-Performance Corrosion-Resistant Iron-Based Amorphous Metal – The Effects of Composition, Structure and Environment on Corrosion Resistance, *Scientific Basis for Nuclear Waste Management XXX*, Symposium NN, MRS Symposium Series, Vol. 985, 2006

[21] T. Lian, D. Day, P. Hailey, J. Choi and J. Farmer, Comparative Study on the Corrosion Resistance of Fe-Based Amorphous Metal, Borated Stainless Steel and Ni-Cr-Mo-Gd Alloy, *Scientific Basis for Nuclear Waste Management XXX*, Symposium NN, MRS Series, Vol. 985, 2006

[22] J. Choi, C. Lee, J. Farmer, D. Day, M. Wall, C. Saw, M. Boussoufi, B. Liu, H. Egbert, D. Branagan, and A. D'Amato, Application of Neutron-Absorbing Structural Amorphous Metal Coatings for Spent Nuclear Fuel Container to Enhance Criticality Safety Controls, *Scientific Basis for Nuclear Waste Management XXX*, Symposium NN, MRS Symposium Series, Vol. 985, 2006

[23] C. Saw, *X-ray Scattering Techniques for Characterization Tools in the Life Sciences, Nanotechnologies for the Life Science*, edited by Challa Kumar, Wiley-VCH Verlag GmbH and Company, KGaA, Weinheim, 2006

[24] C. Saw and R. B. Schwarz, Chemical Short-Range Order in Dense Random-Packed Models, *J. Less-Common Metals*, Vol. 140, 1988, pp. 385-393

[25] K. Gruss, G. Cragnolino, D. Dunn, and N. Sridar, Repassivation Potential for Localized Corrosion of Alloys 625 and C22 in Simulated Repository Environments, Paper 149, Corrosion 98, NACE, Houston, TX, 1998

[26] Standard Reference Test Method for Making Potentiostatic and Potentiodynamic Anodic Polarization Measurements, Designation G 5-94, *1997 Annual Book ASTM Standards,* Section 3, Vol. 3.02, pp. 54–57

[27] R. Treseder, R. Baboian, and C. Munger, Polarization Resistance Method for Determining Corrosion Rates, *Corrosion Engineer's Reference Book*, 2nd Ed., NACE, 1991, pp. 65-66